ICNMM2020-1091

CONTACT LINE PINNING AND DEPINNING PRIOR TO RUPTURE OF AN EVAPORATING DROPLET IN A SIMULATED SOIL PORE

Partha P. Chakraborty, Melanie M. Derby

Department of Mechanical and Nuclear Engineering

Kansas State University Manhattan, KS

ABSTRACT

Altering soil wettability by inclusion of hydrophobicity could be an effective way to restrict evaporation from soil, thereby conserving water resources. In this study, 4-µL sessile water droplets were evaporated from an artificial soil millipore comprised of three glass (i.e. hydrophilic) and Teflon (i.e. hydrophobic) 2.38-mm-diameter beads. The distance between the beads were kept constant (i.e. center-to-center spacing of 3.1 mm). Experiments were conducted in an environmental chamber at an air temperature of 20°C and 30% and 75% relative humidity (RH). Evaporation rates were faster (i.e. ~19 minutes and ~49 minutes at 30% and 75% RH) from hydrophilic pores than the Teflon one (i.e. ~24 minutes and ~52 minutes at 30% and 75% RH) due in part to greater air-water contact area. Rupture of liquid droplets during evaporation was analyzed and predictions were made on rupture based on contact line pinning and depinning, projected surface area just before rupture, and pressure difference across liquid-vapor interface. It was observed that, in hydrophilic pore, the liquid droplet was pinned on one bead and the contact line on the other beads continuously decreased by deforming the liquid-vapor interface, though all three gas-liquid-solid contact lines decreased at a marginal rate in hydrophobic pore. For hydrophilic and hydrophobic pores, approximately 1.7 mm² and 1.8-2 mm² projected area of the droplet was predicted at 30% and 75% RH just before rupture occurs. Associated pressure difference responsible for rupture was estimated based on the deformation of curvature of liquidvapor interface.

Keywords: evaporation, pinning, depinning, hydrophilic, hydrophobic, liquid-vapor interface.

NOMENCLATURE

A	Area (mm²)
CCA	Constant Contact Angle
CCR	Constant Contact Radius
L- V	Liquid vapor

RH	Relative Humidity (%)
T	Temperature (°C)
t	Time (minutes)
P	Pinned contact length (mm)
ΔP	Pressure difference (Pa)
D1, D2, D3	Depinned contact lengths (mm)
Greek letters	
γ	Surface Tension (N/mm)
heta	Contact angle (°)
κ	Curvature (mm ⁻¹)

1. INTRODUCTION

Agriculture is responsible for two-thirds of water withdrawals [1], and faces increasing pressures to produce food for a growing global population. Restricting soil evaporation by introducing hydrophobicity in the soil is an interesting approach to conserve water [2-5]. Shokri et al. [4, 5]experimented with water evaporation from hydrophilic sand column in presence of hydrophobic sand. At 22% *RH*, 25.9 °C, the highest evaporation rate was in 25 mm deep hydrophobic sand column and the lowest was in the 25 mm deep hydrophobic sand and 18 mm hydrophilic/7 mm hydrophobic sand column. Evaporation rates were 50-65% lower in hydrophobic simulated soils than hydrophilic one.

Evaporation of water droplets from hydrophilic and hydrophobic surfaces shows different behavior [6-14]. Concentration gradient during evaporation [6, 11], droplet contact angles and contact areas [7, 10] and gas-liquid-solid contact line pinning and depinning [8, 12-14] were identified as important phenomena during droplet evaporation. Hu and Larson [6] and Erbil [11] noted that, evaporation is a concentration gradient driven phenomenon and the concentration equals the vapor pressure of liquid at given temperature, or difference between saturation and relative humidities. Nguyen et al. [9] experimented on sessile water

droplet evaporation and it was found that evaporation rates were higher in hydrophilic surface than the hydrophobic one.

Birdi and Vu [8] studied evaporation of sessile water droplets from hydrophilic ($\theta < 90^{\circ}$) and hydrophobic ($\theta > 90^{\circ}$) surfaces. On hydrophilic surfaces, droplets were pinned, thereby creating a constant contact radius (CCR) with the surface while the contact angle decreased with time. On the hydrophobic surface, the interfacial contact line of droplet and solid surface decreased continuously during evaporation while the contact angle was constant (CCA). Uno et al. [12] determined evaporating droplets experienced a constant contact radius on hydrophilic surfaces and constant contact angles on hydrophobic surfaces. Yu et al. [13] studied evaporation of water from selfassembled monolayers. Droplet evaporation from hydrophilic surfaces occurred in the constant contact radius mode from the very beginning. According to the research of Fang et al.[14], in smooth hydrophilic surfaces, the droplet was associated with proper wetting accompanied by pinning the gas-liquid-solid contact line. While, in rough surfaces, the droplet experienced dewetting while the gas-liquid-solid contact line decreases with time. Orejon et al. [10] determined the contact line of droplet was pinned initially on hydrophilic surfaces; on hydrophobic surfaces, the contact angle remained steady until the final stage of evaporation.

Change in droplet area associated with two or three beads[15, 16], modeling [17-19] and pressure difference across liquid-vapor contact lines [20-22] were studied to understand and predict droplet rupture. In some studies, the beads were fixed [20, 23-25] while analyzing the rupture phenomena and motion was introduced within the beads in some cases [15, 17, 18] to understand the effect of cohesion force on rupture. Pepin et al. [15] and Darabi et al. [16] experimented with estimation of rupture of liquid bridges between two beads. The rupture was predicted at that point when the area of the liquid bridge would be equal to the areas of two droplets formed at two beads after rupture. Murase et al. [17, 18] and Kruyt et al. [19] estimated the capillary bridge force associated with three and two beads. Equations of liquid-vapor interfacial lines were deduced theoretically and estimation were made on rupture of liquid bridge. Willett et al. [20], Groger et al. [21] and Urso et al. [22] studied liquid bridge (i.e., also called liquid islands) rupture associated with pressure difference estimation in liquid-vapor interfaces. Urso et al. [22] noted the pressure difference across the liquid-vapor interface was directly proportional to the curvature of the interface and they subsequently derived an equation to estimate the increase in pressure difference with increase of curvature. Willett et al. [20] and Groger et al. [21] deduced equations for pressure difference of the liquid-vapor interface associated with two beads. The general form of equation was derived from Laplace-Young equation and it showed proportionality between pressure difference and curvature of the liquid-vapor interface.

The research objectives of this study are to understand contact line motion and rupture of liquid islands during evaporation from a simulated soil pore created with three hydrophilic or hydrophobic beads where the beads are fixed. The rupture of liquid island was predicted on the basis of gas-liquidsolid contact line pinning and depinning, change in projected areas and pressure difference associated with change in curvature along liquid-vapor interface.

2. EXPERIMENTAL APPARATUS

Evaporation of sessile, deionized 4-µL water droplets from simulated soil pores was studied in an environmental chamber (FIGURE 1). Pores were created with three 2.38-mm-diameter, hydrophilic borosilicate glass hydrophobic or polytetrafluoroethylene (PTFE) beads. with a fixed 3.1-mm center-to-center spacing. A fixture was created with additive manufacturing to hold the beads in position and a spacer was used to maintain the constant center-to-center distance. A 4-uL water droplet was placed in the center of three beads with a 0.2-2-µL pipette (Fisherbrand Elite) and since the highest capacity of the pipette is 2-µL, the droplet was deposited twice (2-µL at a time). 2-3% of red food color was applied to the deionized water to get contrast for post-processing of the images.

The experiments were conducted in an environmental chamber. The temperature was maintained at 20°C at atmospheric pressure and two relative humidity levels (i.e. 30% and 75% *RH*) were tested. Evaporation phenomena were captured with a high-speed camera (Fastec IL3) with 5× magnification. The camera recorded the process at 24 frames per second and the evaporation time was determined from videos recorded with Fastmotion. An LED lamp (WD-8W) with magnetic base was used to provide sufficient lighting to the experimental section. The recorded videos were post-processed and analyzed using PFV (Photron FASTCAM Viewer), Active-presenter, and SolidWorks 2018.

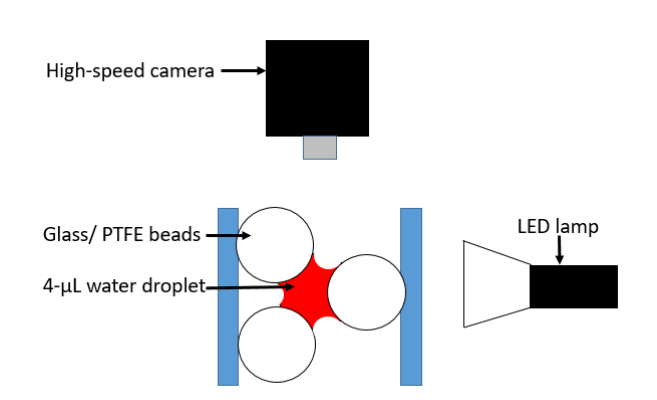


FIGURE 1: SCHEMATIC OF EXPERIMENTAL APPARATUS IN ENVIRONMENTAL CHAMBER

3. RESULTS AND DISCUSSION

Evaporation times (section 3.1), contact line motion (section 3.2), projected area (section 3.3), and analyses of the liquid-vapor interface (section 3.4) are presented in the subsequent sections.

3.1 Evaporation time and liquid island formation

TABLE 1 shows the evaporation time of 4- μ L water droplet from both glass and Teflon pores at RH=30%, 75% and T = 20°C. Each experiment was replicated three times to compare repeatability. The rate of evaporation was faster in glass than Teflon in both relative humidities. Evaporation from glass pores occurred in approximately 19 minutes and 49 minutes at 30% and 75% RH, respectively, compared to 24 minutes and 52 minutes for 30% and 75% RH, respectively. Though, at 30% RH, the evaporation rate at glass was relatively higher than Teflon, but at 75% RH, the evaporation rate difference was less. In glass beads, the droplet was more stretched, thereby creating more airwater contact area which led to faster evaporation rate than Teflon for both 30% and 75% RH.

TABLE 1: TOTAL EVAPORATION TIME FOR BOTH GLASS AND TEFLON PORES AT RH=30% AND 75%, T = 20°C

	Evaporation time (minutes)				
	<i>RH</i> =30%, T = 20°C		RH=75%, T=20°C		
Replication Number	Glass	Teflon	Glass	Teflon	
1	18	24	49	51	
2	18	24	49	53	
3	20	24	49	52	
Average	~19	24	49	52	
time	minutes	minutes	minutes	minutes	

In continuation of evaporation, the whole droplet breaks up and creates a liquid island between two of the beads in order to achieve minimum surface energy. According to Philip and De Vries [26, 27], formation of liquid islands during evaporation played an important role in soil-water evaporation modeling. The analysis of liquid island movement under a temperature gradient was done, while the radii were different as condensation occurred in one side and evaporation occurred in another. In this study, the experiment was conducted in a quiescent atmosphere with no temperature or pressure gradients, resulting in consequent symmetric decrease in radii of liquid island. FIGURE 2 represents liquid island formation in glass and Teflon beads at 75% *RH*. In both cases, the liquid island experienced symmetrical decrease in radii in both sides.

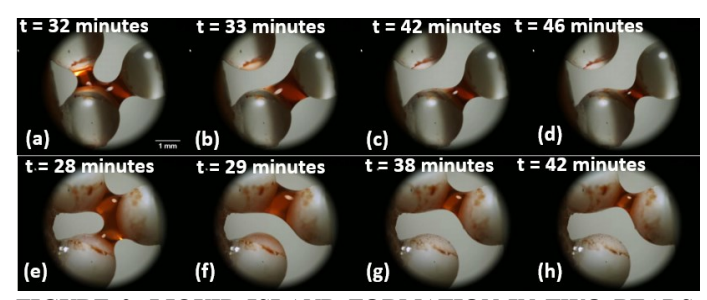


FIGURE 2: LIQUID ISLAND FORMATION IN TWO BEADS. FIGURE (a-d) AND (e-h) SHOW LIQUID ISLAND FORMATION IN TWO BEADS IN GLASS *AND* TEFLON RESPECTIVELY AT 75% *RH*. FIGURE (a) *AND* (e) SHOW THE FINAL STATE OF DROPLET JUST BEFORE RUPTURE

The times of liquid island formation were recorded and analyzed. TABLE 2 shows the time of liquid island formation for both glass and Teflon pores at $T=20^{\circ}\text{C}$, 30 and 75% RH. For 30% RH, liquid island formed earlier in glass beads (i.e. ~8 minutes) than Teflon (i.e. ~13 minutes). But, the phenomena were found different at 75% RH where liquid island formed earlier in Teflon pores (i.e. ~28 minutes) than glass (i.e. ~32 minutes) after rupture of whole droplet while the evaporation rates were nearly similar in glass and Teflon pores at 75% RH. Before rupture of whole droplet, the droplet deforms decreasing the projected surface area and increasing the curvature of liquid-vapor interface. The analysis of these phenomena will be described in next sections.

TABLE 2: TIME OF LIQUID ISLAND FORMATION FOR GLASS AND TEFLON PORES AT RH = 20% AND 75%, T = 20°C

	Time of liquid island formation (minutes)				
	<i>RH</i> =30%, T = 20°C		RH=75%, T = 20°C		
Replication Number	Glass	Teflon	Glass	Teflon	
1	7	11	32	28	
2	7	13	28	23	
3	11	14	36	32	
Average	~8	~13	~32	~28	
time	minutes	minutes	minutes	minutes	

3.2 Contact line pinning and depinning

In this experiment, the water droplet created three contact lines with the solid beads (i.e., glass and Teflon). During evaporation, the droplet changed its shape by changing the contact area and also the contact lines. Images from video files were analyzed on the basis of pinning and depinning of the gasliquid-solid contact lines; the contact lines were measured using Solidworks 2018. To differentiate between the pinned and depinned contact lines, they were measured separately. Since, the contact line pinning and depinning was not similar for same beads in all three replications, the pinned and depinned beads were specified before measuring the contact length. At first, the pinned contact lines were specified by analyzing the images. Then the subsequent depinned contact lines were specified in a clockwise manner.

FIGURE 3 and FIGURE 4 show contact line pinning and depinning in glass and Teflon pores. The gas-liquid-solid contact lines of each bead were measured and plotted at 2 minutes' time interval from the beginning of evaporation till the breakup. In glass beads, the gas-liquid-solid contact lines were found pinned (i.e. the contact lines did not change significantly) in one bead throughout the evaporation and they were depinned (i.e., moving) in the remaining two beads [FIGURE 3 and FIGURE 4 (a, b, c)]. For this analysis, pinned beads (marked as "P") were first identified and the other two depinned beads (Marked as D1 and D2) were labeled in a clockwise manner.

In Teflon pores all the gas-liquid-solid contact lines decreased in the three beads. In Teflon pores, the bead that

experienced sharpest decrease rate in contact length was specified as "Depinned 1" and other two beads were specified as "Depinned 2" and "Depinned 3" in a clockwise manner (FIGURE 3 and FIGURE 4 (d, e, f)). This is consistent with the findings of Birdi and Vu [8], Uno et al. [12], Yu et al. [13], which noted that during evaporation of sessile water droplet from flat hydrophilic and hydrophobic surfaces, the droplet contact lines did not change in hydrophilic surface while it decreased in hydrophobic surface.

Per FIGURE 3 and at 30% RH, in the glass pore the pinned contact length did not change throughout the evaporation (i.e. \sim 2 mm) and the remaining two contact lengths decreased gradually. Rupture occurred in that bead which experienced lowest contact length before breakup (marked as D1). In the Teflon pore, all the three contact lengths experienced gradual decrease from the beginning till the breakup of the whole droplet and the bead with lowest contact length (marked as D1) was associated with droplet rupture.

At 75% RH, the glass pore experienced one pinned gasliquid-solid contact length (marked as "P") with an estimated length of ~2.1 mm. This contact length did not change significantly with respect to time while the remaining two contact lengths (marked as D1 and D2) decreased gradually during evaporation (FIGURE 4). For Teflon pore, the gas-liquidsolid contact lines in all three beads (marked as D1, D2 and D3) decreased from very beginning of the evaporation until the rupture of whole droplet.

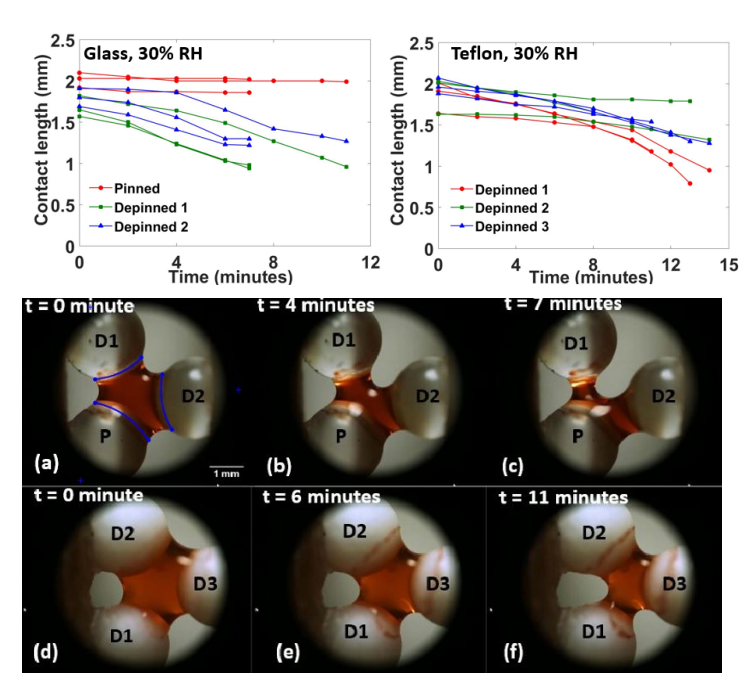


FIGURE 3: CONTACT LINE PINNING AND DEPINNING OF GLASS AND TEFLON AT 30% RH. THE PLOTS REPRESENT THE CHANGE IN CONTACT LENGTH IN GLASS AND TEFLON. FIG. a, b, c AND d, e, f REPRESENT THE CONTACT LINE PINNING AND DEPINNING IN GLASS AND TEFLON PORES RESPECTIVELY. P, D1, D2 AND D3 REPRESENT PINNED, DEPINNED 1, DEPINNED 2 AND DEPINNED 3 BEADS

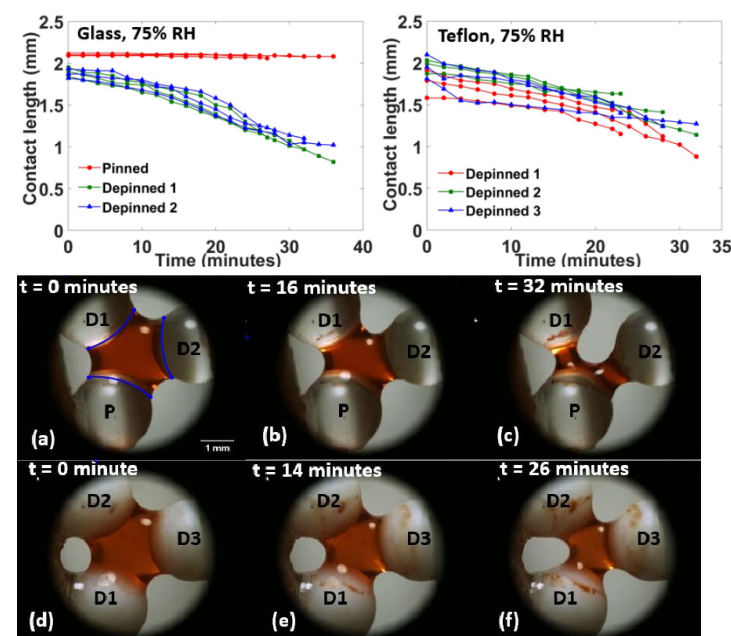


FIGURE 4: CONTACT LINE PINNING AND DEPINNING OF GLASS AND TEFLON AT 75% RH. THE PLOTS REPRESENT THE CHANGE IN CONTACT LENGTH IN GLASS AND TEFLON. Fig. a,b,c AND d,e,f REPRESENT THE CONTACT LINE PINNING AND DEPINNING IN GLASS AND TEFLON PORES RESPECTIVELY. P, D1, D2, D3 REPRESENT PINNED, DEPINNED 1, DEPINNED 2 AND DEPINNED 3 RESPECTIVELY

3.3 Projected area

The evaporation phenomena were captured with a highspeed camera located vertically on the top of the test section, hence the projected areas were calculated based on the areas of whole droplet from top-view images. Figure 5(a) and 5(g) show the actual projected areas from top-view projection. In Solidworks 2018, the droplet was redrawn with accurate pixel size and by "area measurement" tools, the areas of the droplet were measured at 2 minute's interval. The projected area of whole droplet continually decreased during evaporation. FIGURE 5 (a-c) and FIGURE 5 (d-f) show the projected area decrease in glass and Teflon pores respectively at 30% RH, while FIGURE 5 (g-i) and FIGURE 5 (j-l) show the change in projected area in glass and Teflon pores at 75% RH. The initial projected area was found a bit larger in Teflon (i.e., ~3.11 mm² and $\sim 3.89 \text{ mm}^2$ at 30% and 75% RH) than glass (i.e., $\sim 3.01 \text{ mm}^2$ and ~3.11 mm² at 30% and 75% RH) and it decreased simultaneously with time. The rate of decrease in projected area was larger in glass than Teflon at both relative humidities. Since, glass is hydrophilic, the water droplet likely created a larger airwater contact area.

Projected areas were measured just before the breakup. At 30% RH, the projected areas before breakup were similar in glass and Teflon pores (i.e. \sim 1.75 mm² for glass and \sim 1.69 mm² for Teflon). At 75% RH, the final projected areas were found \sim 1.81 mm² for glass and \sim 2.13 mm² for Teflon.

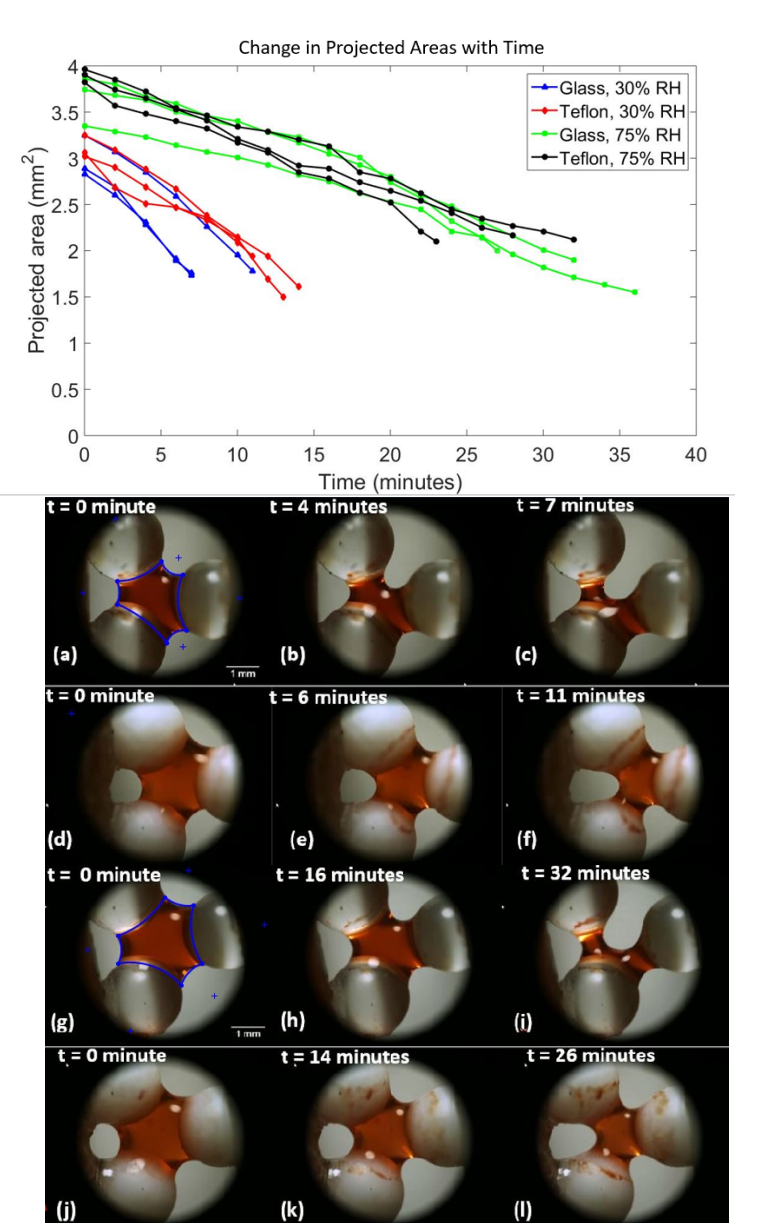


FIGURE 5: THE PLOT REPRESENTS THE CHANGE IN PROJECTED AREA DURING EVAPORATION. FIGURES a,b,c AND g,h,i SHOW THE PROJECTED AREA CHANGE IN GLASS PORES AT 30% AND 75% RH RESPECTIVELY. FIGURES d,e,f AND j,k,l SHOW THE CHANGE IN PROJECTED AREA IN TEFLON PORE AT 30% AND 75% AT DIFFERENT TIMES

After breakup of whole droplet, the liquid created a liquid island between two beads. After formation of liquid island between two beads, there was still some water present in the third bead. In a two bead system, Pepin et al. [15] predicted that rupture occurred when liquid-vapor area of the liquid island, $A_{LV-bridge}$, was equal to liquid-vapor area of the two droplet formed in two beads, $A_{LV-droplets}$ (i.e., surface energy minimization). The equation was stated as follows:

$$A_{LV-droplets} - A_{LV-bridge} = 0 (1)$$

In this experiment, the rupture of whole droplet was predicted and after rupture the projected area of liquid island and liquid droplet formed in the other bead were measured. According to the previous equation, the liquid island projected area should be equal to the area of the liquid droplet in the other bead. FIGURE 6 represents the liquid droplet formed in one bead and liquid island formed in two beads just after the breakup of whole droplet. The projected area calculation of liquid droplet just before rupture and after rupture (i.e. total areas of liquid droplet formed in one bead and liquid island in two beads) is shown in TABLE 3. The projected areas were measured using Solidworks 2018 and the areas before and after breakup showed significant similarities with highest +6.67% and lowest of -1.3% deviation

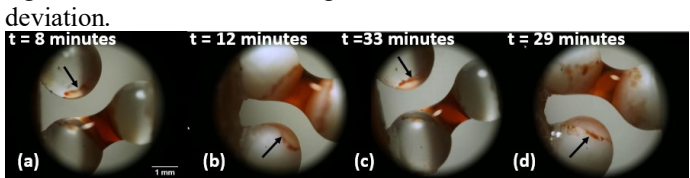


FIGURE 6: LIQUID DROPLET FORMED IN ONE BEAD (ARROW SIGN) AND LIQUID ISLAND FORMED IN TWO BEADS AFTER BREAKUP OF WHOLE DROPLET IN GLASS AND TEFLON PORES AT 30% (a,b) AND 75% RH (c,d)

TABLE 3: PERCENTAGE OF DEVIATION IN DROPLET PROJECTED AREAS BEFORE RUPTURE AND TOTAL AREAS AFTER RUPTURE

30% <i>RH</i> , glass						
	Area before rupture (mm²)	Area in one bead after rupture (mm²)	Area in two beads after rupture (mm²)	Total area after rupture (mm²)	Deviation	
Replication 1	1.73	0.32	1.38	1.7	-1.73%	
Replication 2	1.76	0.21	1.53	1.74	-1.13%	
Replication 3	1.78	0.32	1.38	1.7	-4.49%	
30% RH, Teflon						
Replication 1	1.94	0.3	1.6	1.9	-2.06%	
Replication 2	1.5	0.33	1.27	1.6	+6.67%	
Replication 3	1.61	0.3	1.24	1.54	-4.34%	
75% RH, glass						
Replication 1	1.9	0.55	1.3	1.85	-2.63%	

Replication 2	2	0.39	1.55	1.94	-3%	
Replication 3	1.55	0.51	0.97	1.48	-4.52%	
75% <i>RH</i> , Teflon						
Replication 1	2.17	0.58	1.55	2.13	-1.84%	
Replication 2	2.1	0.4	1.8	2.2	+4.76%	
Replication 3	2.12	0.52	1.57	2.09	-1.42%	

3.4 Liquid-vapor interface

The rupture of whole droplet is associated with the pressure difference across the liquid-vapor interface. During evaporation, contact line pinning and depinning occurs, resulting in significant changes in curvature of liquid-vapor interface line. According to Urso et al.[22], the pressure difference across the liquid-vapor interface in a capillary liquid bridge is governed by Laplace-Young equation when the gravitational force is negligible,

 $\kappa = \frac{\Delta P}{\gamma} \tag{2}$

where, κ is the curvature of the meniscus profile, γ is the surface tension of liquid and ΔP is the pressure difference across the liquid-vapor interface.

In these experiments, the droplet was spread among three glass or Teflon beads, creating three liquid-gas and three gasliquid-solid interfaces. Observing all the replications, it was found that one liquid-vapor interface typically changed more than the remaining two, and that created subsequent rupture of whole droplet. After exporting images at 2 minutes' interval, the particular liquid-vapor interfaces were detected for all replications which were susceptible to deform much. Then, with "curvature tool" of SolidWorks 2018, the curvature of the liquidvapor interface was measured. It was found that, initially, the particular liquid-vapor interface looked like an arc with constant curvature. But it transformed into elliptical or parabolic shape around 4-6 minutes before rupture. In that case, the maximum curvature of the liquid-vapor interface was measured and all the curvatures were plotted against time from the initial of evaporation till before breakup of whole droplet (FIGURE 7 and FIGURE 8).

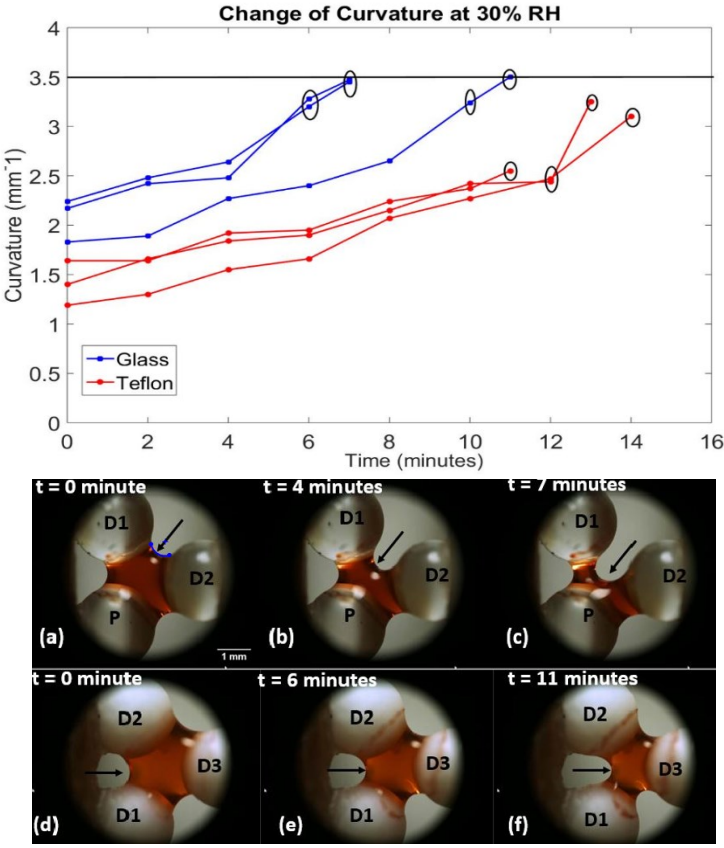
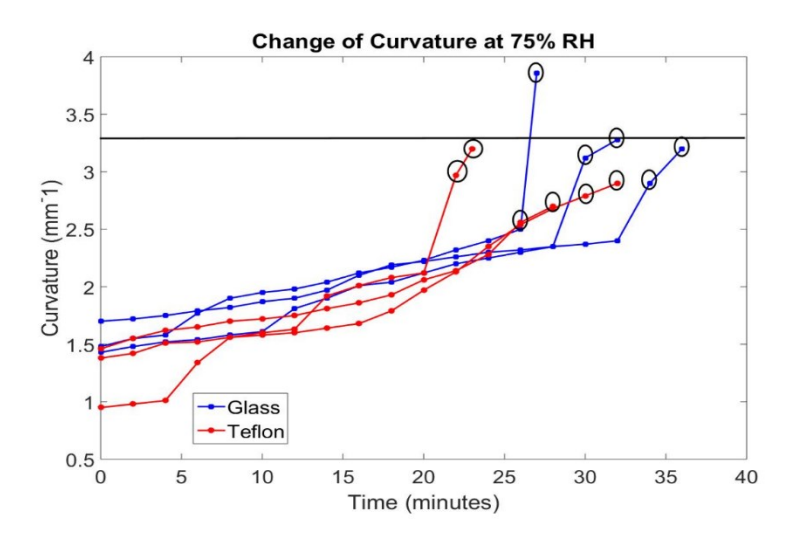


FIGURE 7: CHANGE OF CURVATURE IN LIQUID-VAPOR INTERFACE AT 30% *RH*. a,b,c *AND* d,e,f SHOW THE CURVATURE CHANGE (ARROW SIGN) IN GLASS *AND* TEFLON PORES, RESPECTIVELY. THE ELLIPTICAL MARKS REPRESENT THE TRANSFORMATION OF LIQUID-VAPOR INTERFACE FROM ARC TO PARABOLIC SHAPE



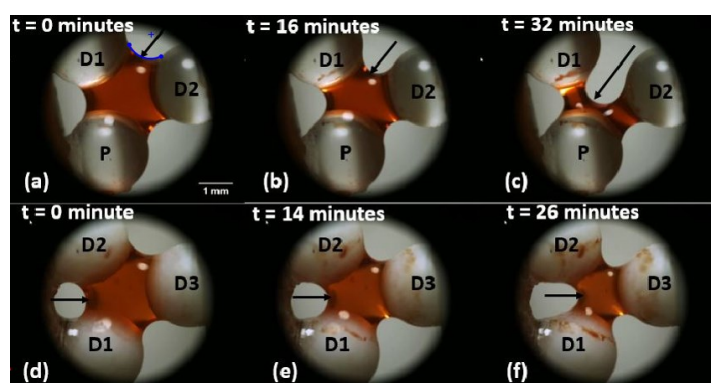


FIGURE 8: CHANGE OF CURVATURE IN LIQUID-VAPOR INTERFACE AT 75% RH. a,b,c AND d,e,f SHOW THE CURVATURE CHANGE (ARROW SIGN) IN GLASS AND TEFLON PORES, RESPECTIVELY. THE ELLIPTICAL MARKS REPRESENT THE TRANSFORMATION OF LIQUID-VAPOR INTERFACE FROM ARC TO PARABOLIC SHAPE

FIGURE 7 and FIGURE 8 represent the change in liquidvapor curvature at 30% and 75% RH for both glass and Teflon. The plots show that, from the beginning of evaporation to droplet breakup, the curvature of liquid-vapor interface increased with time for both glass and Teflon. Initially, the liquid-vapor interface looked like an arc with constant curvature (FIGURE 7 and FIGURE 8 (a, b, d, e), but it transformed into a parabolic/elliptical shape before rupture (FIGURE 7 and FIGURE 8 (c, f). In that case, the maximum curvature was measured. The elliptical marks on the graph represent the points where the liquid-vapor interface started deforming from arc into parabolic shape ~4-6 minutes before breakup. The maximum curvature was found ~3.5 mm⁻¹ and ~3.2-4 mm⁻¹ for glass and \sim 3 mm⁻¹ and \sim 2.7-3.1 mm⁻¹ for Teflon at 30% and 75% RH respectively just before breakup. As, the pressure difference across liquid-vapor interface is proportional to curvature, it can be approximated that, the pressure difference needed to initiate rupture was higher in glass than Teflon.

4. CONCLUSIONS

This paper investigated the evaporation dynamics of $4-\mu L$ water droplet from a simulated soil pore created with three hydrophilic glass or three hydrophobic Teflon beads. The following conclusions can be drawn based on this research:

- The evaporation rate was faster in glass pores than Teflon pores at both 30% and 75% *RH*, though the difference in evaporation rate was modest in glass and Teflon at 75% *RH*.
- The gas-liquid-solid contact lines were pinned in one bead in glass and they decreased in the remaining two beads, while all the gas-liquid-solid contact lines decreased in Teflon from beginning until the breakup of liquid droplet at both 30% and 75% RH.
- The projected areas were decreased in both glass and Teflon pores at 30% and 75% RH. The ultimate projected

- area just before rupture was \sim 1.7 mm² at 30% *RH* and \sim 1.8-2 mm² at 75% for both glass and Teflon.
- The area before the droplet breakup and total areas of liquid droplet formed in one bead and liquid bridge formed between two beads after breakup was found almost similar with highest +6.67% and lowest of -1.3% deviation
- The curvature of the liquid-vapor interface prior to rupture was found increasing in glass and Teflon pores from beginning of evaporation till breakup at both 30% and 75% *RH*. The ultimate curvature of liquid-vapor interface just before breakup was found higher in glass than Teflon at both 30% and 75% *RH*.

ACKNOWLEDGEMENTS

The authors gratefully acknowledge the support of NSF CAREER grant number 1651451 and NSF grant number 1828571.

REFERENCES

- [1] Oki, T., and Kanae, S., 2006, "Global hydrological cycles and world water resources," science, 313(5790), pp. 1068-1072.
- [2] Bachmann, J., Woche, S., Goebel, M. O., Kirkham, M., and Horton, R., 2003, "Extended methodology for determining wetting properties of porous media," Water resources research, 39(12).
- [3] Davis, D. D., Horton, R., Heitman, J. L., and Ren, T., 2014, "An experimental study of coupled heat and water transfer in wettable and artificially hydrophobized soils," Soil Science Society of America Journal, 78(1), pp. 125-132.
- [4] Shokri, N., Lehmann, P., and Or, D., 2008, "Effects of hydrophobic layers on evaporation from porous media," Geophysical Research Letters, 35(19).
- [5] Shokri, N., Lehmann, P., and Or, D., 2009, "Characteristics of evaporation from partially wettable porous media," Water Resources Research, 45(2).
- [6] Hu, H., and Larson, R. G., 2002, "Evaporation of a sessile droplet on a substrate," The Journal of Physical Chemistry B, 106(6), pp. 1334-1344.
- [7] Deegan, R. D., Bakajin, O., Dupont, T. F., Huber, G., Nagel, S. R., and Witten, T. A., 2000, "Contact line deposits in an evaporating drop," Physical review E, 62(1), p. 756.
- [8] Birdi, K., Vu, D., and Winter, A., 1989, "A study of the evaporation rates of small water drops placed on a solid surface," The Journal of physical chemistry, 93(9), pp. 3702-3703.
- [9] Nguyen, T. A., Nguyen, A. V., Hampton, M. A., Xu, Z. P., Huang, L., and Rudolph, V., 2012, "Theoretical and experimental analysis of droplet evaporation on solid surfaces," Chemical engineering science, 69(1), pp. 522-529.
- [10] Orejon, D., Sefiane, K., and Shanahan, M. E., 2011, "Stick—slip of evaporating droplets: substrate hydrophobicity and nanoparticle concentration," Langmuir, 27(21), pp. 12834-12843.

- [11] Erbil, H. Y., 2012, "Evaporation of pure liquid sessile and spherical suspended drops: A review," Advances in colloid and interface science, 170(1-2), pp. 67-86.
- [12] Uno, K., Hayashi, K., Hayashi, T., Ito, K., and Kitano, H., 1998, "Particle adsorption in evaporating droplets of polymer latex dispersions on hydrophilic and hydrophobic surfaces," Colloid and polymer science, 276(9), pp. 810-815.
- [13] Yu, H. Z., Soolaman, D. M., Rowe, A. W., and Banks, J. T., 2004, "Evaporation of Water Microdroplets on Self-Assembled Monolayers: From Pinning to Shrinking," ChemPhysChem, 5(7), pp. 1035-1038.
- [14] Fang, X., Pimentel, M., Sokolov, J., and Rafailovich, M., 2010, "Dewetting of the three-phase contact line on solids," Langmuir, 26(11), pp. 7682-7685.
- [15] Pepin, X., Rossetti, D., Iveson, S. M., and Simons, S. J., 2000, "Modeling the evolution and rupture of pendular liquid bridges in the presence of large wetting hysteresis," Journal of colloid and interface science, 232(2), pp. 289-297.
- [16] Darabi, P., Li, T., Pougatch, K., Salcudean, M., and Grecov, D., 2010, "Modeling the evolution and rupture of stretching pendular liquid bridges," Chemical Engineering Science, 65(15), pp. 4472-4483.
- [17] Murase, K., Mochida, T., and Sugama, H., 2004, "Experimental and numerical studies on liquid bridge formed among three spheres," Granular Matter, 6(2-3), pp. 111-119.
- [18] Murase, K., Mochida, T., Sagawa, Y., and Sugama, H., 2008, "Estimation on the strength of a liquid bridge adhered to three spheres," Advanced Powder Technology, 19(4), pp. 349-367.
- [19] Kruyt, N. P., and Millet, O., 2017, "An analytical theory for the capillary bridge force between spheres," Journal of fluid mechanics, 812, pp. 129-151.
- [20] Willett, C., Adams, M., Johnson, S., and Seville, J., 2003, "Effects of wetting hysteresis on pendular liquid bridges between rigid spheres," Powder Technology, 130(1-3), pp. 63-69.
- [21] Gröger, T., Tüzün, U., and Heyes, D. M., 2003, "Modelling and measuring of cohesion in wet granular materials," Powder Technology, 133(1-3), pp. 203-215.
- [22] Urso, M. E. D., Lawrence, C. J., and Adams, M. J., 1999, "Pendular, funicular, and capillary bridges: Results for two dimensions," Journal of colloid and interface science, 220(1), pp. 42-56.
- [23] De Bisschop, F. R., and Rigole, W. J. J., 1982, "A physical model for liquid capillary bridges between adsorptive solid spheres: The nodoid of plateau," Journal of Colloid Interface Science
- 88(1), pp. 117-128.
- [24] Simons, S., Seville, J., and Adams, M. J., 1994, "An analysis of the rupture energy of pendular liquid bridges," Chemical Engineering Science, 49(14), pp. 2331-2339.
- [25] Chakraborty, P. P., Huber, R., Chen, X., and Derby, M. M., 2018, "EVAPORATION FROM SIMULATED SOIL PORES: EFFECTS OF WETTABILITY, LIQUID ISLANDS, AND BREAKUP," J Interfacial Phenomena Heat Transfer, 6(4).

[26] Philip, J., and De Vries, D., 1957, "Moisture movement in porous materials under temperature gradients," Eos, Transactions American Geophysical Union, 38(2), pp. 222-232. [27] De Vries, D., 1958, "Simultaneous transfer of heat and moisture in porous media," Eos, Transactions American Geophysical Union, 39(5), pp. 909-916.